HHS Public Access

Author manuscript

Exp Eye Res. Author manuscript; available in PMC 2022 May 01.

Published in final edited form as:

Exp Eye Res. 2021 May ; 206: 108540. doi:10.1016/j.exer.2021.108540.

Retinal hypoxia and angiogenesis with methamphetamine

Minsup Lee, **Wendy Leskova**, **Randa S. Eshaq**, **Norman R. Harris***

Department of Molecular & Cellular Physiology, Louisiana State University Health Shreveport Shreveport, LA 71103

Abstract

Central retinal artery occlusion, retinopathy, and retinal neovascularization have been reported in methamphetamine (METH) abusers. In the current study, we investigated whether METH induces retinal neovascularization in a mouse model, and if so, whether the neovascularization is associated with increased hypoxia, hypoxia-inducible factor 1α (HIF-1α), and vascular endothelial growth factor (VEGF). Mice were administrated METH by intraperitoneal injection over a 26-day period, or injected with saline as a vehicle control. The number of retinal arterioles and venules were counted using *in vivo* live imaging following infusion with fluorescein isothiocyanate-dextran. Excised retinas were stained with griffonia simplicifolia lectin I and flat mounted for a measurement of vascularity (length of vessels per tissue area) with AngioTool. Retinal hypoxia was examined by formation of pimonidazole (Hypoxyprobe) adducts with anti-pimonidazole antibody, and HIF-1α and VEGFa protein levels in the retina were detected by immunoblot. METH administration increased vascularity (including the number of arterioles) measured on Day 26. Retinal VEGFa protein level was not changed in METH-treated mice on Day 5, but was increased on Day 12 and Day 26. Hypoxia (pimonidazole adduct formation) was increased in retinas of METH-treated mice on Day 12 and Day 26, as were HIF-1α protein expression levels. These results indicate that METH administration induces hypoxia, HIF-1α, VEGFa, and angiogenesis in the retina.

Keywords

Methamphetamine; hypoxia; angiogenesis; HIF-1α; VEGF

1. Introduction

One of the actions of methamphetamine (METH) is to modulate the release of neurotransmitters, including that of dopamine through inhibition of reuptake. Low doses of METH are prescribed for treatment of attention-deficit/hyperactivity disorder; however,

*Corresponding author: Norman R. Harris, Ph.D., Professor & Chair, Department of Molecular & Cellular Physiology/LSU Health Shreveport, 1501 Kings Highway, Shreveport, LA 71130, Phone: 318-675-6013, Fax: 318-675-6005, nharr6@lsuhsc.edu.

Competing interests

The author(s) declare no competing interests.

increased release of neurotransmitters by METH is associated with an induction of a feeling of euphoria, causing addiction (Kiyatkin and Sharma, 2016; Riddle et al., 2006). Since the neurotransmitters regulated by METH administration play roles in the central nervous and cardiovascular systems, the misuse or overdose of METH contributes to neurodegenerative and cardiovascular pathologies including ischemic brain injuries and damage to the heart (Al-Zubaidi et al., 2020; Darke et al., 2019; Kevil et al., 2019; Merchant et al., 2019; Ng and Chong, 2018). According to the Key Substance Use and Mental Health Indicators in the United States report (Substance Abuse and Mental Health Services Administration, 2019), in 2018, approximately 1.9 million people age 12 or older used METH and 205,000 people age 12 or older began METH use in the United States. An estimated 1.1 million people age 12 or older had a METH use disorder in 2018. Among them, an estimated 899,000 adults age 26 or older are possible chronic users, with this number increasing dramatically from the estimated 539,000 adults in 2016.

Ischemic injuries in several tissues including the heart, brain, liver, and retina have been reported in METH abusers (Al-Zubaidi et al., 2020; Anderson and Sung, 2003; Darke et al., 2019; Merchant et al., 2019; Ng and Chong, 2018; Wei et al., 2018). The monoamine neurotransmitters dopamine, serotonin, and norepinephrine, which are increased by METH, are vasoconstrictors involved in the regulation of blood pressure and blood flow. The effects of these neurotransmitters on platelet aggregation (Anfossi et al., 1992; Cerrito et al., 1993; Vlachakis and Aledort, 1979) are considered to contribute to occlusive diseases (Jenkins et al., 1975), which could be associated with the pathologic mechanisms of METH-induced ischemia. In a mouse model of METH administration, we have previously found decreases in retinal endothelial glycocalyx molecules, syndecan-1 and glypican-1 (Lee et al., 2020), with the loss of glycocalyx potentially contributing to leukocyte/platelet adhesion to the retinal microvasculature.

Hypoxia following ischemia stimulates neovascularization, in most cases via the activation of vascular endothelial growth factor (VEGF) (Hurst, 2016; Lin et al., 2011). Hypoxia-inducible factor 1-alpha (HIF-1α), a subunit of the HIF-1 transcription factor, is stabilized in response to low tissue oxygen levels, and regulates expression of more than 60 genes including VEGF (Hurst, 2016). Angiogenesis induced by increased VEGF via hypoxia-activated HIF-1α is an important pathway in retinal degenerative diseases such as diabetic retinopathy (Lin et al., 2011; Penn et al., 2008), but whether this pathway contributes to METH-induced retinal angiogenesis has yet to be investigated. Recently, METH-induced retinopathy with neovascularization and retinal vascular occlusions has been documented in a case report of a METH abuser (Guo et al., 2019). We hypothesize that the retinal angiogenic response will occur in a mouse model of METH administration that was designed to mimic human use, in a binge-and-crash pattern (Kesby et al., 2018), and moreover that the retinal angiogenesis will be accompanied by increases in hypoxia, HIF-1α, and VEGF.

2. Materials and methods

2.1 Animals and drug administration

C57BL/6 male mice (8 weeks old, Jackson Laboratory, Raleigh, NC) were used. All animals were treated in accordance with the Association for Research in Vision and Ophthalmology Statement for the Use of Animals in Ophthalmic and Vision Research. The animal protocol was approved by the Animal Care and Use Committee at LSU Health Sciences Center in Shreveport. The animals were housed in cages with free access to food and water. Temperature and humidity in the animal facility were controlled at 23±1°C and 53±15%, respectively. The mice received intraperitoneal injections (4 times per day with 2 hour intervals) with progressively increasing doses of METH (0–6 mg/kg; Table 1) or bacteriostatic saline as a vehicle in a method similar to that described previously in mice to model human use patterns (Kesby et al., 2018). After the final injection of METH, total body weights of mice in both saline- and METH-treated groups tended to decrease, although not statistically significant (Table 2).

2.2 Whole retinal flatmount and quantitative analysis of retinal vascular networks

Within 30 min after the last METH injection, mice were anesthetized intraperitoneally with a ketamine/xylazine cocktail (100 mg/kg and 10 mg/kg, respectively), and the eye was immediately enucleated and washed with phosphate-buffered saline (PBS), with the eye fixed in 4% paraformaldehyde (v/v) for 1 h. Retinas were separated, permeabilized, and blocked with 0.5% Triton X-100, 5% goat serum, and 0.3% bovine serum albumin in PBS for 1 h. The retinas were then incubated in fluorescein-conjugated griffonia simplicifolia lectin I (GSL-1) (Vector Laboratories, Burlingame, CA) for 1 h at room temperature. After washing three times in tris-buffered saline with Tween 20, sections were mounted with Fluoromount-G (SouthernBiotech, Birmingham, AL) mounting solution, and fluorescent images of mid-peripheral and peripheral retina were captured with a fluorescent microscope (Nikon, Tokyo, Japan). To determine retinal angiogenesis, retinal vasculature stained with GSL-1 was analyzed with AngioTool (Zudaire et al., 2011). The average vascular length density (length of vessels per unit area) of 4 different selected explant areas from each retina was used for analysis.

2.3 Surgery and preparation for intravital microscopy

Perfusion of the retinal circulation was observed *in vivo* with intravital microscopy. For this procedure, mice were anesthetized intraperitoneally with a ketamine/xylazine cocktail. An incision was made along the shaved lower abdomen, and the femoral vein was cannulated with polyethylene tubing (PE10) filled with heparinized saline (25 U/ml). The mice were kept warm on a heating pad for the remainder of the experiment and both eyes were moistened with PBS. Prior to intravital microscopy, the pupil of the left eye was dilated with a drop of Tropicamide Ophthalmic Solution USP 1% (Falcon Pharmaceuticals.; Ft. Worth, TX) followed with one drop of Gonak™ Hypromellose Ophthalmic Demulcent Solution, 2.5% (Akorn; Lake Forest, IL), with the eye then covered with a five-mm circular glass coverslip. Fluorescein isothiocyanate (FITC)-dextran infusion through the femoral vein allowed the identification of the retinal arterioles (filling first) and venules (filling last).

2.4 Immunoblot analysis

Excised retinas were lysed by RIPA buffer (Thermo Fisher Scientific, Waltham, MA) for preparation of whole protein lysates. After incubation on ice for 20 min, and centrifugation at 10,000g for 20 min, the supernatant was collected and kept at −80°C until used. Protein concentrations in the supernatants were determined by bicinchoninic acid assay (Thermo Fisher Scientific). Aliquots of protein were denatured with Laemmle sample buffer (Bio-Rad, Hercules, CA) containing 2.5% β-mercaptoethanol (Bio-Rad) for 10 min at 100°C. Equal volumes of protein were separated by sodium dodecyl sulfate-polyacrylamide gel electrophoresis and transferred onto a nitrocellulose membrane. The membrane was then blocked with protein-free T20 blocking solution (Thermo Fisher Scientific) for 1 h. The membranes were incubated with primary antibodies (HIF-1α and VEGFa, abcam, Cambridge, CA). The primary antibodies of HIF-1α and VEGFa were diluted in TBST to 1:500 (v/v) and 1:1,000 (v/v), respectively. The blots were treated with horseradish peroxidase conjugated goat anti-rabbit IgG or anti-mouse IgG secondary antibodies (1:10,000 in TBST (v/v), Jackson ImmunoResearch Laboratories, West Grove, PA) for 2 h, and immune complexes were detected using Clarity western enhanced chemiluminescence substrate (Bio-Rad). Densitometric analysis of the data obtained from at least three independent experiments was performed using a ChemiDoc Image acquisition system (Bio-Rad) and ImageJ (v1.52a, NIH, Bethesda, MD). Relative levels of protein expression were normalized with β-actin (Santa Cruz Biotechnology, Dallas, TX) detected from the same membrane.

2.5 Retinal hypoxia

To examine retinal hypoxia, a Hypoxyprobe kit (Hypoxyprobe, Burlington, MA) was used as described in the manufacturer's protocol. Briefly, the mice were administrated with 60 mg/kg of pimonidazole hydrochloride by intraperitoneal injection. After 4 h, as a positive control, the left common carotid artery (CCA) was exposed through a midline cervical incision under anesthesia, with the CCA tied with silk suture for occlusion (CCAO). The right CCA was also exposed, but remained unoccluded to serve as a contralateral control. The incision was thereafter closed with a suture. After 30 min, the eyes were collected. For the METH protocol, the mice were injected with 60 mg/kg of pimonidazole hydrochloride for 4 h before anesthesia, with the eyes collected under anesthesia just prior to euthanasia. One retina was lysed in RIPA for whole protein extraction and the other fixed in 4% paraformaldehyde (v/v) for whole retinal flatmounts. Retinal levels of hypoxia were analyzed by the formation of pimonidazole adducts with a specific primary antibody detected on the nitrocellulose membrane and in whole retinal flatmounts. The relative level of pimonidazole adducts was normalized by total protein level measured with REVERT Total Protein Stain kit (LI-COR Biosciences, Lincoln, NE).

2.6 Statistics

Statistical analyses were performed using GraphPad Prism (GraphPad, La Jolla, CA) software. Student *t*-tests were used to compare the group means. All data are presented as mean ± standard error, with $*P < 0.05$ considered statistically significant.

3. Results

To identify the effect of METH on retinal vascularity, the fixed retina was stained with GSL-1 and total retinal vascular length per unit area was analyzed with AngioTool (Fig 1). The vessel length density of mid-peripheral retina (Fig 1A) in the METH-treated group at Day 5 (47.6±2.4 mm/mm^2, number (N)=3) and Day 12 (52.2±1.0 mm/mm^2, N=5) were not significantly different from the saline-treated group at Day 5 (46.9±2.1 mm/mm^2, N=3) and Day 12 (49.9±1.2 mm/mm^2, N=5). However, the vessel length density at Day 26 was significantly increased by METH administration (55.8±1.5 mm/mm^2, P<0.05, N=5), compared with saline-treated group (47.7±2.1 mm/mm^2, N=5). The vessel length density of the peripheral retina (Fig 1B) was also significantly increased by METH administration at Day 26 (43.7±0.4 mm/mm^2, P<0.001, N=4), compared with the saline-treated group (40.5±0.3 mm/mm^2, N=4). The vessel length densities of the peripheral retina were not changed by METH administration at Day 5 (39.7±0.6 vs 39.9±0.8 mm/mm^2, N=3) or Day 12 (40.4±0.3 vs 40.6±0.6 mm/mm^2, N=3).

We additionally quantified the number of perfused retinal arterioles and venules using intravital microscopy with an infusion of FITC-dextran through the femoral vein. The number of venules did not change due to METH administration at Day 26 (an average of 5.3 venules/retina in both METH and control groups). However, as shown in Fig 2, the average number of arterioles per venule increased from a value of 1.02 ± 0.02 (N=7) in controls to 1.22 ± 0.05 with METH (N=7; p<0.01) at Day 26. In 6/7 control mice, the number of arterioles was equal to the number of venules; however, in 6/7 METH mice, the number arterioles exceeded the number of venules.

We also examined the protein expression level of retinal VEGFa, which is a key mediator of retinal and choroidal angiogenic diseases among the VEGF family. At Day 5, the protein expression level of VEGFa in the retina was not changed in the METH-treated group compared with the control group (Fig 3A). However, retinal VEGFa protein expression in the METH-treated group was significantly increased 2.4-fold (N=5, p<0.05) at Day 12 (Fig 3B) and 3.1-fold (N=6–8, p<0.05) at Day 26 (Fig 3C), compared with controls, indicating that METH administration elevates retinal VEGF levels.

Low tissue oxygen in the retina stimulates VEGF signaling and promotes vascularization (Penn et al., 2008). To determine the extent of retinal hypoxia, we quantified the level of pimonidazole adducts formed in the retina, with and without METH administration. As a positive control, the detection of pimonidazole adduct formation under hypoxia in the retina was confirmed by the immune reaction of the primary pimonidazole antibody with whole retinal protein lysates (Fig 4A) and using a retinal flatmount (Fig 4B) after common carotid artery occlusion for 30 min. As shown in Fig 5, the formation of pimonidazole adducts in the retina was significantly increased 2.9-fold (N=3, p<0.05) by METH administration at Day 12 (Fig 5B), compared with the control group. At Day 26 (Fig 6), pimonidazole adduct formation was also significantly increased 5.8-fold (N=4, p<0.01) with METH administration, compared with the control group (Fig 6B). In retinal flatmounts, the immunoreactivities of pimonidazole adducts (red) were increased in the retinas of METH

mice at Day 12 (Fig 5C) and Day 26 (Fig 6C), compared with the control groups, indicating METH-induced retinal hypoxia.

With the finding of METH-induced retinal hypoxia, we further examined the retinal protein expression level of HIF-1α, which is activated by tissue hypoxia. As shown in Fig 7, the protein expression level of HIF-1α in the METH retina was significantly increased 2.3-fold ($N=5$, $p<0.001$) at Day 12 (Fig 7A and B) and 5.3-fold ($N=8$, $p<0.001$) at Day 26 (Fig 7C and D) compared with the control groups.

4. Discussion

Long-term METH users have been reported to have the ocular consequences of CRAO, ischemic retinopathy, and retinal neovascularization (Anderson and Sung, 2003; Guo et al., 2019), with the mechanisms of METH-induced retinal angiogenesis yet to be explored. In this study, we found that the retinas of mice treated with METH for 26 days showed evidence of retinal angiogenesis with an increased number of arterioles and vascular density. We also found increased retinal hypoxia in mice given METH for 12 and 26 days, with the METH-induced retinal hypoxia the likely stimulus for retinal angiogenesis, with potential disadvantages for retinal function. As a highly metabolic tissue, the retina requires a constant vascular supply; however, a dense vascular network anterior to the photoreceptors would interfere with light absorption, with the outer retina receiving most of its oxygen from the choroid. Regression of retinal capillaries occurs in oxygen-induced (hyperoxia) retinopathy animal models (Iizuka et al., 2015), with subsequent retinal neovascularization following restoration of normoxia (Madan and Penn, 2003).

Retinal blood flow is an important determinant of inner retinal oxygenation, as shown by oxygen tensions near 0 mmHg in the inner retina following laser-induced occlusion of the retinal microcirculation (Yu et al., 2007). The retinal vasculature is vulnerable to METH-induced complications, with ocular manifestations of METH including retinal vasculitis, vasoconstriction, ischemia, and occlusion of the CRA (Anderson and Sung, 2003; Guo et al., 2019; Hazin et al., 2009; Kumar et al., 2006; Shaw et al., 1985; Wijaya et al., 1999), with the CRA responsible for supplying the inner retina. Lack of blood supply by the CRAO typically presents an acute visual loss (Cugati et al., 2013), but also causes neovascularization (Mason et al., 2015). Moreover, ocular neovascularization occurs up to 2 years after the CRAO diagnosis (Mason et al., 2015). Occlusions can occur due to platelet and leukocyte adhesion leading to thrombi, with these adhesive events in some circumstances enabled by loss of the endothelial glycocalyx. In our previous study, we found a METH-induced loss of the endothelial glycocalyx molecules syndecan-1 and glypican-1 from the retina and CRA (Lee et al., 2020).

Irrespective of occlusive events, retinal blood flow may decrease with METH administration through vasoconstriction. Although we did not measure either retinal blood flow rate or occlusion events in our mice administered with METH, a group of patients who used METH prior to traumatic brain injuries showed decreased cerebral blood flow (O'Phelan et al., 2013), and an *in vivo* study with acute METH administration in C57BL/6 mice has shown a decrease of cerebral blood flow (Polesskaya et al., 2011). Extrapolation of these previous

reports could suggest that lower blood flow rate with METH administration might cause retinal hypoxia, which is present in our METH mouse model.

HIF-1α, a transcriptional regulator for angiogenic genes including VEGF, is an oxygen sensor (Wang and Semenza, 1993). In normal oxygen levels, HIF-1α is ubiquitously degraded by hydroxylation of its proline residues. However, with low oxygen, the pathway of HIF-1α degradation is suppressed and cellular protein levels of HIF-1α are increased (Hurst, 2016; Wang and Semenza, 1993). Our findings of increased levels of HIF-1α protein in the retina of METH-treated mice at Day 12 and Day 26 are consistent with the measurements of retinal hypoxia induced by METH. Once HIF-1α is activated, it promotes the expression of target genes such as VEGF. The mechanism of hypoxia inducing increases in HIF-1α and VEGF, which then stimulates angiogenesis, is well-established in retinal degenerative diseases including retinopathy of prematurity, aged-related macular degeneration, and diabetic retinopathy, which are leading causes of visual loss. Suppression of HIF-1α decreases retinal VEGF levels and neovascularization in an *in vivo* oxygen-induced retinopathy model (Lin et al., 2011), which mimics retinopathy of prematurity and diabetic retinopathy. With increased HIF-1α in the retina following administration of METH for 12 and 26 days in our current study, levels of VEGF were substantially elevated.

VEGF signaling regulates endothelial proliferation and vascular development. The growth factor has a major role in retinal neovascularization in retinal degenerative diseases and therefore, anti-VEGF therapies are used to suppress retinal neovascularization and recover visual function (Tah et al., 2015). In addition, VEGF is associated with a loss of barrier proteins, and increases of adhesion molecules and matrix metalloproteinases (Lee et al., 2017). Moreover, VEGF is a chemoattractant for leukocytes, including monocytes and macrophages (Nakao et al., 2012), via the VEGF receptor 1 (Sawano et al., 2001). With its ability to promote monocyte/macrophage infiltration into the retina, excessive levels of VEGF are also associated with retinal inflammation (Lee et al., 2017; Penn et al., 2008). Anti-VEGF antibody treatment reduces leukocyte trafficking in the retina (Nakao et al., 2012), which could suppress retinal inflammation. It is possible that the elevation of VEGF in the retina following METH administration may play a major pathogenic role in METH-induced retinal angiogenesis and retinopathy.

In conclusion, we observed METH-induced retinal angiogenesis (increased numbers of arterioles and vascular density), with associated increases in hypoxia, HIF-1α, and VEGF. To our knowledge, this is the first study of *in vivo* retinal hypoxia and angiogenesis by chronic METH administration. The mechanisms of hypoxia/HIF-1α/VEGF by METH may represent a potential target for addressing METH-induced retinopathy.

Acknowledgements

We would like to thank Dr. Christopher Pattillo and his lab members for providing the ChemiDoc XRS gel imaging system, and for guidance with the system.

Funding

This work was supported by funding from the National Institute of Health (NIH) EY025632.

Abbreviations

CCA	Common carotid artery
CCAO	common carotid artery occlusion
CRA	central retinal artery
CRAO	central retinal artery occlusion
FITC	Fluorescein isothiocyanate
GSL-1	griffonia simplicifolia lectin I
HIF-1α	Hypoxia-inducible factor 1-alpha
METH	methamphetamine
PBS	phosphate-buffered saline
PECAM-1	platelet endothelial cell adhesion molecule-1
VEGF	vascular endothelial growth factor

References

Al-Zubaidi M, Stuart A, Jayaratne T, Marsdin E, 2020. Non-surgical management of methamphetamine induced testicular ischemia. Urol. Case Rep 32, 101238. 10.1016/j.eucr.2020.101238. [PubMed: 32420042]

Anderson CA, Sung GY, 2003. Central retinal artery occlusion associated with intranasal methamphetamine use. J. Stroke Cerebrovasc. Dis 12, 207–208. 10.1016/S1052-3057(03)00073-9. [PubMed: 17903928]

Anfossi G, Massucco P, Mularoni E, Cavalot F, Burzacca S, Mattiello L, Trovati M, 1992. Studies on the effect of dopamine on the human platelet response. Clin. Exp. Pharmacol. Physiol 19, 613–618. 10.1111/j.1440-1681.1992.tb00513.x. [PubMed: 1382907]

Cerrito F, Lazzaro MP, Gaudio E, Arminio P, Aloisi G, 1993. $5HT_2$-receptors and serotonin release: their role in human platelet aggregation. Life Sci. 53, 209–215. 10.1016/0024-3205(93)90671-o. [PubMed: 8321084]

Cugati S, Varma DD, Chen CS, Lee AW, 2013. Treatment options for central retinal artery occlusion. Curr. Treat. Options. Neurol 15, 63–77. 10.1007/s11940-012-0202-9. [PubMed: 23070637]

Darke S, Duflou J, Kaye S, Farrell M, Lappin J, 2019. Psychostimulant use and fatal stroke in young adults. J. Forensic Sci 64, 1421–1426. 10.1111/1556-4029.14056. [PubMed: 30941776]

Guo J, Tang W, Liu W, Zhang Y, Wang L, Wang W, 2019. Bilateral methamphetamine-induced ischemic retinopathy. Am. J. Ophthalmol. Case Rep 15, 100473. 10.1016/j.ajoc.2019.100473. [PubMed: 31194074]

Hazin R, Cadet JL, Kahook MY, Saed D, 2009. Ocular manifestations of crystal methamphetamine use. Neurotox. Res 15, 187–191. 10.1007/s12640-009-9019-z. [PubMed: 19384581]

Hurst JH, 2016. William Kaelin, Peter Ratcliffe, and Gregg Semenza receive the 2016 Albert Lasker Basic Medical Research Award. J. Clin. Invest 126, 3628–3638. 10.1172/JCI90055 [PubMed: 27620538]

Iizuka N, Nakahara T, Ushikubo H, Mori A, Sakamoto K, Ishii K, 2015. Retinal region-dependent susceptibility of capillaries to high-concentration oxygen exposure and vascular endothelial growth factor receptor inhibition in neonatal mice. J. Pharmacol. Sci 129, 107–118. 10.1016/j.jphs.2015.08.010. [PubMed: 26403253]

Jenkins CD, Thomas G, Olewine D, Zyzanski SJ, Simpson MT, Hames CG, 1975. Blood platelet aggregation and personality traits. J. Human Stress 1, 34–46. 10.1080/0097840X.1975.9939551.

Kesby JP, Chang A, Markou A, Semenova S, 2018. Modeling human methamphetamine use patterns in mice: chronic and binge methamphetamine exposure, reward function and neurochemistry. Addict. Biol 23, 206–218. 10.1111/adb.12502. [PubMed: 28224681]

Kevil CG, Goeders NE, Woolard MD, Bhuiyan MS, Dominic P, Kolluru GK, Arnold CL, Traylor JG, Orr AW, 2019. Methamphetamine use and cardiovascular disease. Arterioscler. Thromb. Vasc. Biol 39, 1739–1746. 10.1161/ATVBAHA.119.312461. [PubMed: 31433698]

Kiyatkin EA, Sharma HS, 2016. Breakdown of blood-brain and blood-spinal cord barriers during acute methamphetamine intoxication: role of brain temperature. CNS Neurol. Disord. Drug Targets 15, 1129–1138. 10.2174/1871527315666160920112445. [PubMed: 27658516]

Kumar RL, Kaiser PK, Lee MS, 2006. Crystalline retinopathy from nasal ingestion of methamphetamine. Retina. 26, 823–824. 10.1097/01.iae.0000244275.03588.ad. [PubMed: 16963858]

Lee M, Leskova W, Eshaq RS, Harris NR, 2020. Acute changes in the retina and central retinal artery with methamphetamine. Exp. Eye. Res 193, 107964. 10.1016/j.exer.2020.107964. [PubMed: 32044305]

Lee M, Yun S, Lee H, Yang J, 2017. Quercetin mitigates inflammatory responses induced by vascular endothelial growth factor in mouse retinal photoreceptor cells through suppression of nuclear factor kappa B. Int. J. Mol. Sci18, 2497. 10.3390/ijms18112497.

Lin M, Chen Y, Jin J, Hu Y, Zhou KK, Zhu M, Le YZ, Ge J, Johnson RS, Ma JX, 2011. Ischaemia-induced retinal neovascularisation and diabetic retinopathy in mice with conditional knockout of hypoxia-inducible factor-1 in retinal Muller cells. Diabetologia. 54, 1554–1566. 10.1007/s00125-011-2081-0. [PubMed: 21360191]

Madan A, Penn JS, 2003. Animal models of oxygen-induced retinopathy. Front. Biosci 8, d1030–1043. 10.2741/1056. [PubMed: 12700061]

Mason JO 3rd, Patel SA, Feist RM, Albert MA Jr., Huisingh C, McGwin G Jr., Thomley ML, 2015. Ocular neovascularization in eyes with a central retinal artery occlusion or a branch retinal artery occlusion. Clin. Ophthalmol 9, 995–1000. 10.2147/OPTH.S82796. [PubMed: 26089631]

Merchant K, Schammel C, Fulcher J, 2019. Acute Methamphetamine-Induced Hepatic and Pancreatic Ischemia. Am. J. Forensic Med. Pathol 40, 285–288. 10.1097/PAF.0000000000000486. [PubMed: 31033491]

Nakao S, Arima M, Ishikawa K, Kohno R, Kawahara S, Miyazaki M, Yoshida S, Enaida H, Hafezi-Moghadam A, Kono T, Ishibashi T, 2012. Intravitreal anti-VEGF therapy blocks inflammatory cell infiltration and re-entry into the circulation in retinal angiogenesis. Invest. Ophthalmol. Vis. Sci 53, 4323–4328. 10.1167/iovs.11-9119. [PubMed: 22661475]

Ng CF, Chong CY, 2018. Methamphetamine-induced internal carotid artery vasospasm: A rapidly fatal stroke. Neurol. India 66, 826–827. 10.4103/0028-3886.232337. [PubMed: 29766948]

O'Phelan K, Ernst T, Park D, Stenger A, Denny K, Green D, Chang C, Chang L, 2013. Impact of methamphetamine on regional metabolism and cerebral blood flow after traumatic brain injury. Neurocrit. Care 19, 183–191. 10.1007/s12028-013-9871-9. [PubMed: 23836426]

Penn JS, Madan A, Caldwell RB, Bartoli M, Caldwell RW, Hartnett ME, 2008. Vascular endothelial growth factor in eye disease. Prog. Retin. Eye Res 27, 331–371. 10.1016/j.preteyeres.2008.05.001. [PubMed: 18653375]

Polesskaya O, Silva J, Sanfilippo C, Desrosiers T, Sun A, Shen J, Feng C, Polesskiy A, Deane R, Zlokovic B, Kasischke K, Dewhurst S, 2011. Methamphetamine causes sustained depression in cerebral blood flow. Brain Res. 1373, 91–100. 10.1016/j.brainres.2010.12.017. [PubMed: 21156163]

Riddle EL, Fleckenstein AE, Hanson GR, 2006. Mechanisms of methamphetamine-induced dopaminergic neurotoxicity. AAPS J. 8, E413–418. 10.1007/BF02854914. [PubMed: 16808044]

Sawano A, Iwai S, Sakurai Y, Ito M, Shitara K, Nakahata T, Shibuya M, 2001. Flt-1, vascular endothelial growth factor receptor 1, is a novel cell surface marker for the lineage of monocyte-macrophages in humans. Blood 97, 785–791. 10.1182/blood.v97.3.785. [PubMed: 11157498]

Shaw HE Jr., Lawson JG, Stulting RD, 1985. Amaurosis fugax and retinal vasculitis associated with methamphetamine inhalation. J. Clin. Neuroophthalmol 5, 169–176. 10.3109/01658108509079659. [PubMed: 2934418]

Substance Abuse and Mental Health Services Administration, 2019. Key substance use and mental health indicators in the United States: Results from the 2018 National Survey on Drug Use and Health (HHS Publication No. PEP19–5068, NSDUH Series H-54) Rockville, MD.

Tah V, Orlans HO, Hyer J, Casswell E, Din N, Sri Shanmuganathan V, Ramskold L, Pasu S, 2015. Anti-VEGF therapy and the retina: An update. J. Ophthalmol 2015, 627674. 10.1155/2015/627674. [PubMed: 26417453]

Vlachakis ND, Aledort L, 1979. Platelet aggregation in relationship to plasma catecholamines in patients with hypertension. Atherosclerosis. 32, 451–460. 10.1016/0021-9150(79)90011-x. [PubMed: 465125]

Wang GL, Semenza GL, 1993. General involvement of hypoxia-inducible factor 1 in transcriptional response to hypoxia. Proc. Natl. Acad. Sci. U. S. A 90, 4304–4308. 10.1073/pnas.90.9.4304. [PubMed: 8387214]

Wei GL, Zheng XZ, Chen KQ, Shi YY, Wang LY, Tan XY, 2018. Coronary sinus flow is reduced in methamphetamine abusers: a transthoracic echocardiographic study. Int. J. Cardiovasc. Imaging 34, 1889–1894. 10.1007/s10554-018-1417-y. [PubMed: 30032415]

Wijaya J, Salu P, Leblanc A, Bervoets S, 1999. Acute unilateral visual loss due to a single intranasal methamphetamine abuse. Bull. Soc. Belge Ophtalmol 271, 19–25. [PubMed: 10355156]

Yu DY, Cringle SJ, Yu PK, Su EN, 2007. Intraretinal oxygen distribution and consumption during retinal artery occlusion and graded hyperoxic ventilation in the rat. Invest. Ophthalmol. Vis. Sci 48, 2290–2296. 10.1167/iovs.06-1197. [PubMed: 17460293]

Zudaire E, Gambardella L, Kurcz C, Vermeren S, 2011. A computational tool for quantitative analysis of vascular networks. PLoS One. 6, e27385. 10.1371/journal.pone.0027385. [PubMed: 22110636]

Highlights

- Chronic methamphetamine administration induces retinal angiogenesis in mice.
- Methamphetamine causes retinal hypoxia.
- Methamphetamine activates HIF-1α/VEGF signaling in the retina.

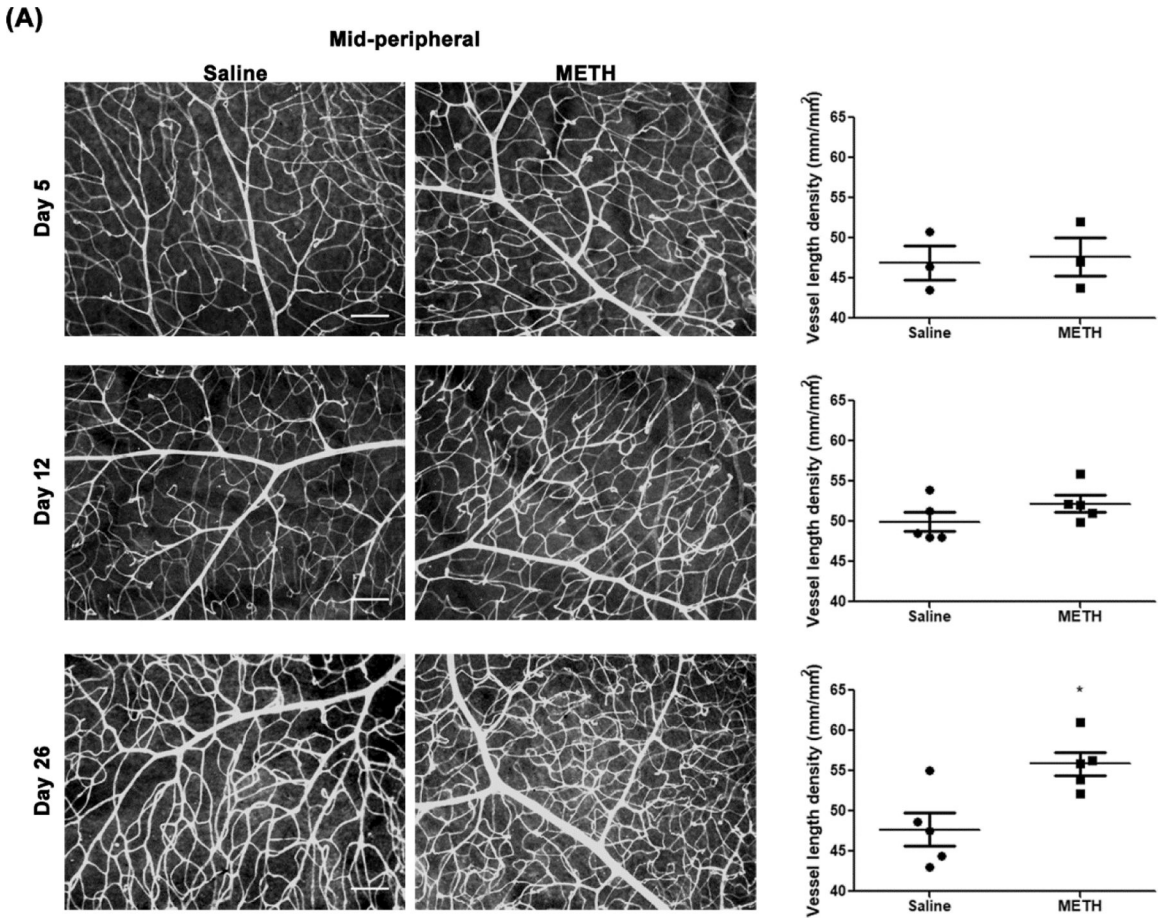

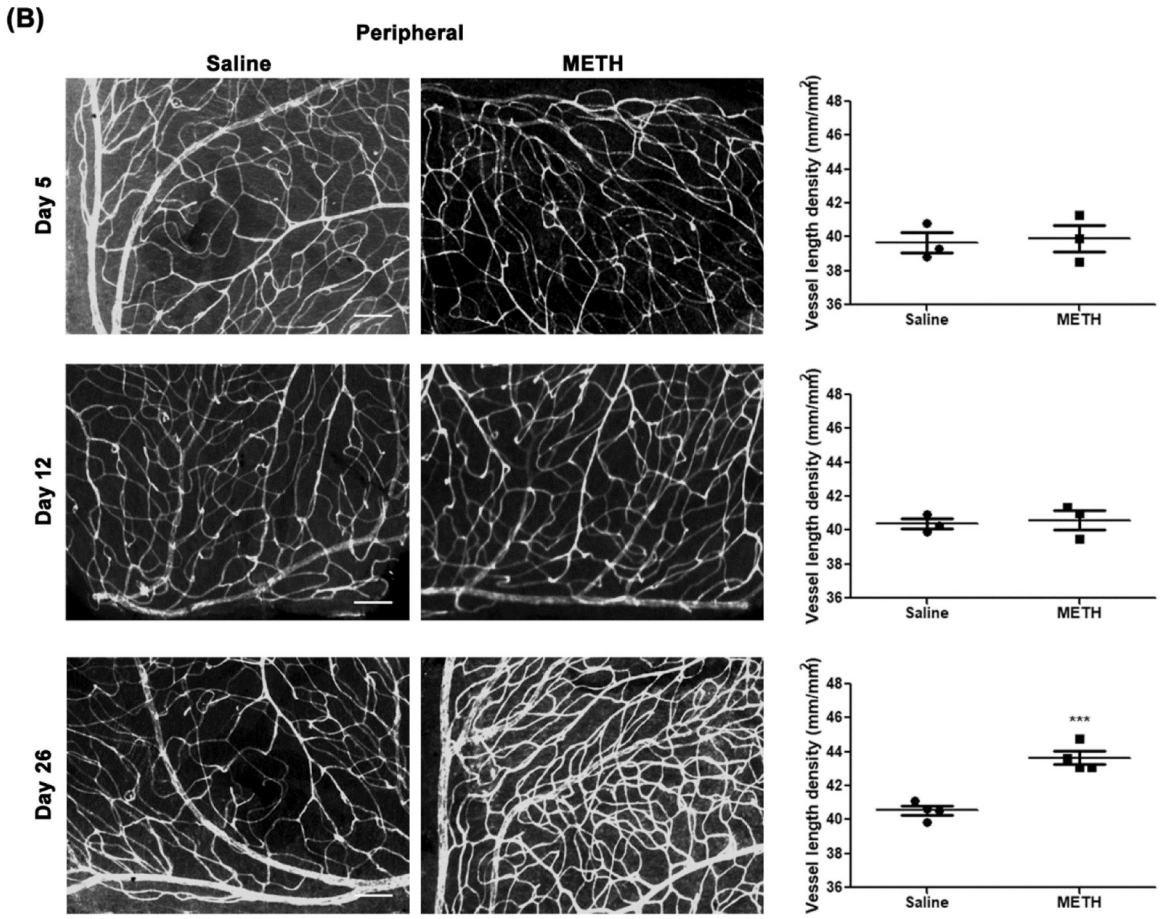

Figure 1.

Effect of METH on retinal vascularity. Fixed eyes were stained with GSL-1 and flat mounted for microscopic photographs. Graphs provide total retinal blood vessel length per unit area as measured by AngioTool, with N=3–5 per group. Panels A, mid-peripheral retina; B, peripheral retina. Scale bar = 100 μm. *p<0.05 and ***p<0.001 vs saline-injected controls.

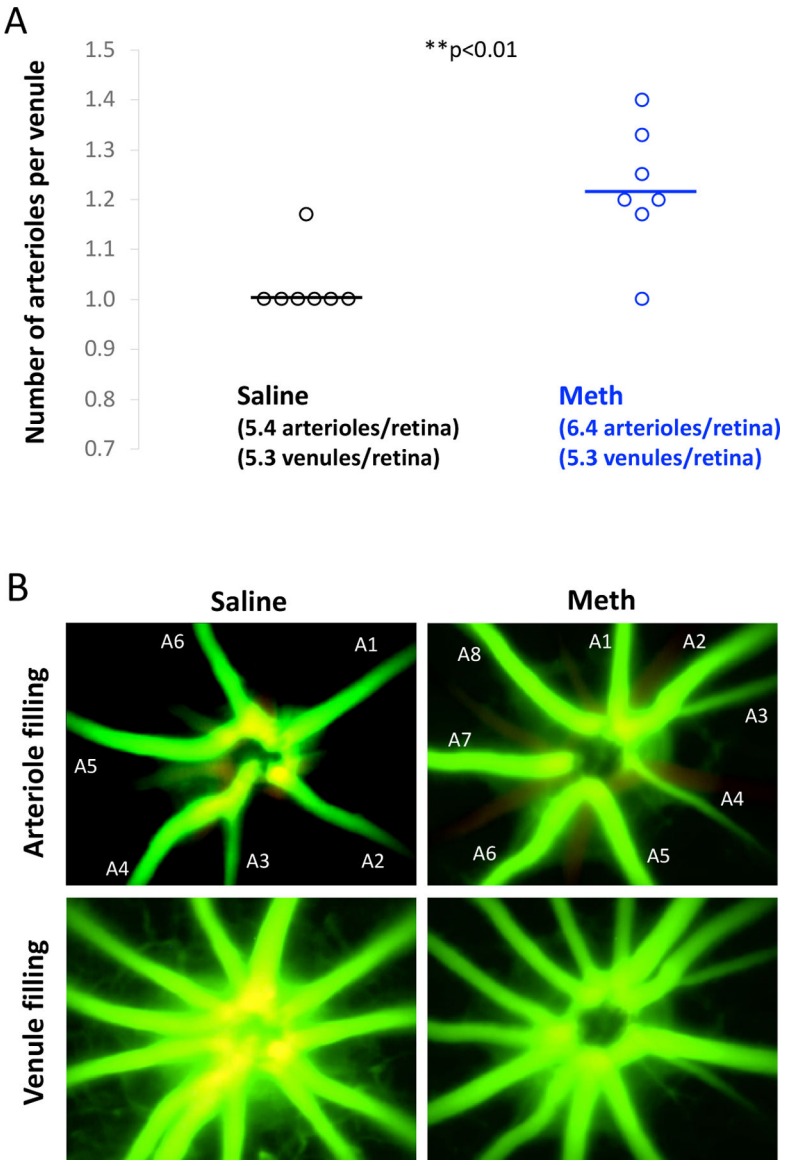

Figure 2.

A. Number of retinal arterioles per venule in control (saline-) and METH-injected mice at Day 26. N=7 per group. **p<0.01. B. Example of arteriolar and venular filling of fluorescent dye to determine the number of primary arterioles (filling first; numbered A1-A7) and venules (filling subsequently).

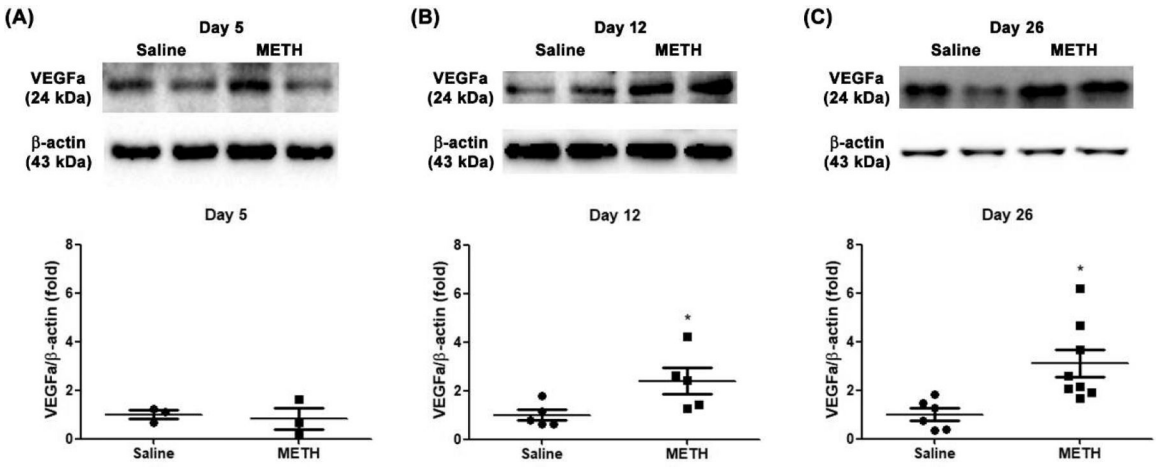

Figure 3.

Effect of METH on protein expression of VEGFa in the retina. VEGFa protein expression in the retina at Day 5 (A, N=3 per group), Day 12 (B, N=5 per group), and Day 26 (C, N=6–8 per group) was examined by immunoblot. The relative protein expression level of VEGFa was normalized to β-actin expression using ImageJ. *$p<0.05$ vs saline-injected controls.

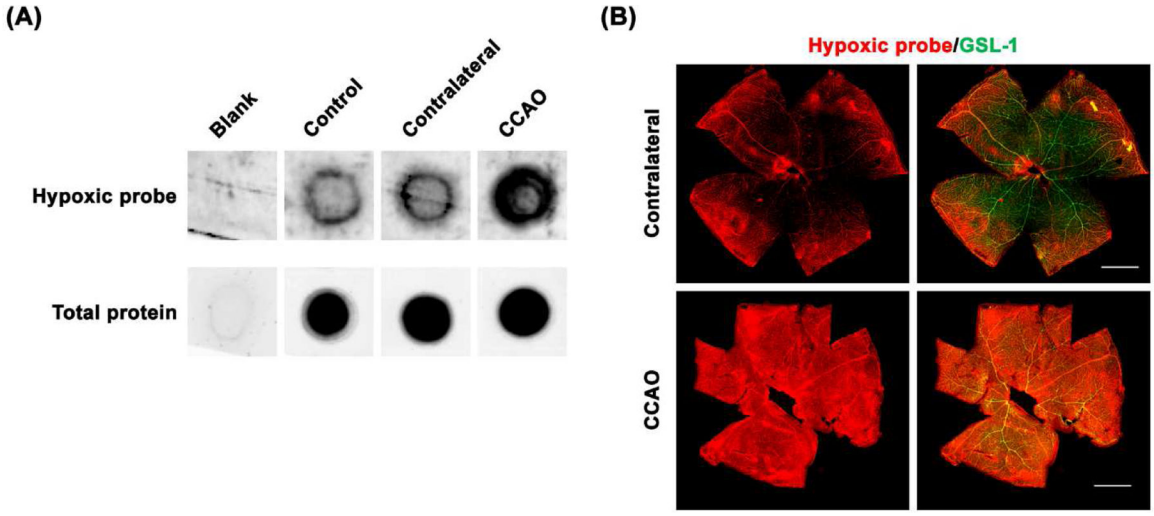

Figure 4.

Detection of retinal hypoxia. As a positive control, retinal hypoxia induced by CCAO in mice was detected with formation of pimonidazole (Hypoxyprobe) adducts in retinal lysates on nitrocellulose membranes (A). The fixed eyes were stained with Hypoxyprobe primary antibody (red) and GSL-1 (green) and dissected and flat mounted for microscopic photographs (B).

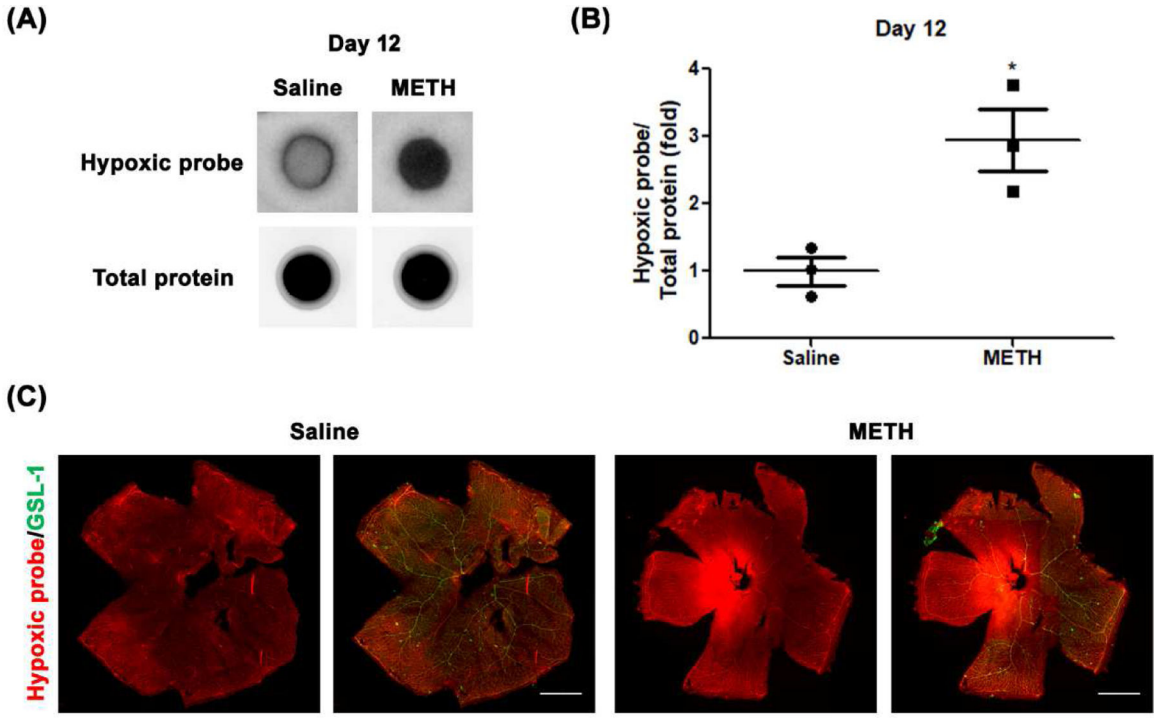

Figure 5.

Effect of METH on hypoxia in the retina at Day 12. Pimonidazole (Hypoxyprobe) adducts from retina whole lysates were detected on nitrocellulose membrane (A). The relative pimonidazole adduct level was normalized to total protein using Image J (B). *$p<0.05$ vs saline-injected controls; N=3. The fixed eyes were stained with Hypoxyprobe primary antibody (red) and GSL-1 (green) and dissected and flat mounted for microscopic photographs (C). Scale bar = 1 mm.

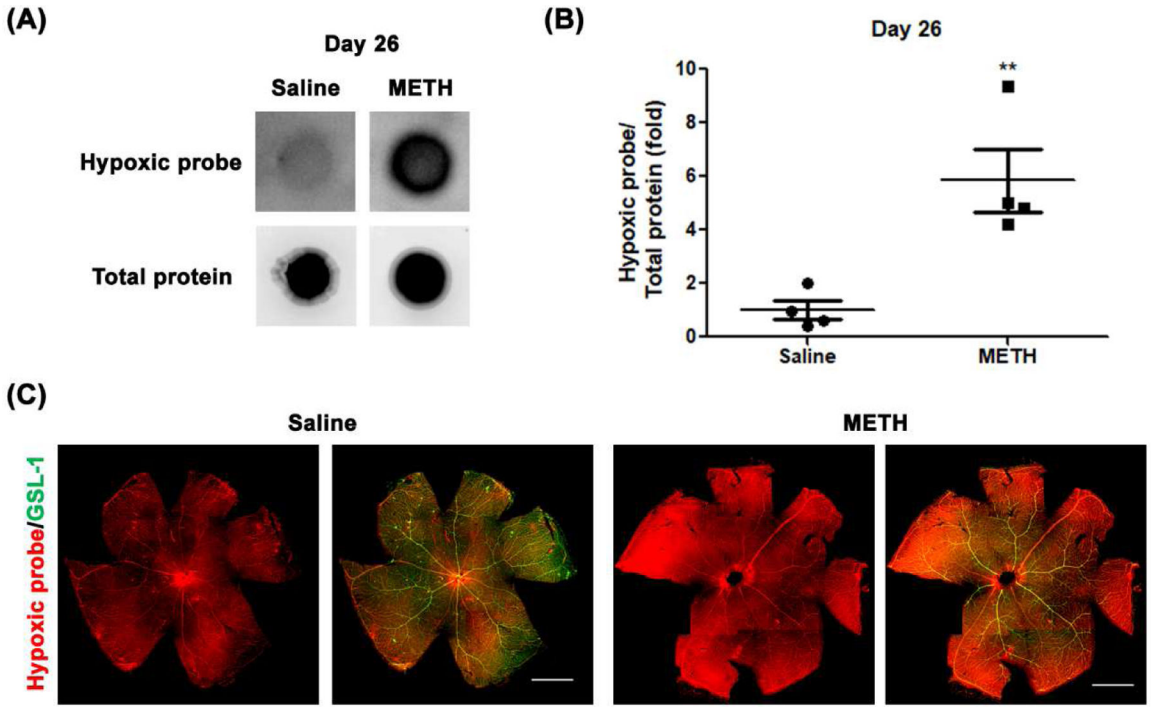

Figure 6.

Effect of METH on hypoxia in the retina at Day 26. Pimonidazole (Hypoxyprobe) adducts from retina whole lysates were detected on nitrocellulose membrane (A). The relative pimonidazole adduct level was normalized to total protein using Image J (B). *p<0.05 vs saline-injected controls; N=4. The fixed eyes were stained with Hypoxyprobe primary antibody (red) and GSL-1 (green) and dissected and flat mounted for microscopic photographs (C). Scale bar = 1 mm.

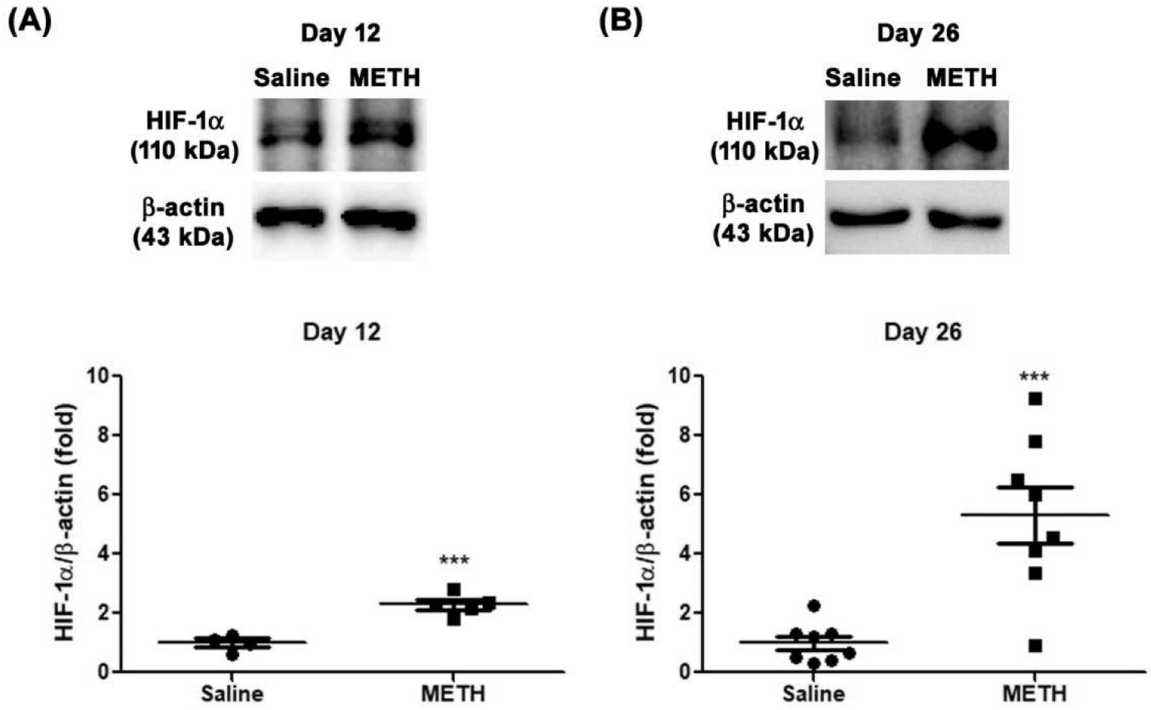

Figure 7.

Effect of METH on protein expression of HIF-1α in the retina, examined by immunoblot. The relative protein expression level of HIF-1α was normalized to β-actin expression using ImageJ. (A) Day 12 (N=5), (B) Day 26 (N=8). ***P < 0.001 vs saline-injected controls.

Table 1.

Schedule of methamphetamine administration of four injections per day over an approximate four-week period.

Day	METH (mg/kg)			
	1	**2**	**3**	**4**
1	0	0	0	0
2	1	1	2	2
3	3	3	4	4
4	5	5	5	5
5	6	6	6	6
6	-	-	-	-
7	-	-	-	-
8	0	0	0	0
9	3	3	4	4
10	5	5	5	5
11	6	6	6	6
12	6	6	6	6
13	-	-	-	-
14	-	-	-	-
15	0	0	0	0
16	3	3	4	4
17	5	5	5	5
18	6	6	6	6
19	6	6	6	6
20	-	-	-	-
21	-	-	-	-
22	0	0	0	0
23	3	3	4	4
24	5	5	5	5
25	6	6	6	6
26	6	6	6	6

Table 2.

Animal information

		Total body weight (g) Saline	
		Saline	**METH**
I	Day 0 (N=3)	29.1±0.8	28.8±0.6
	Day 5 (N=3)	28.7±0.7	28.0±0.7
II	Day 0 (N=8)	29.1±0.6	29.0±0.8
	Day 12 (N=8)	27.2±0.5	27.6±0.4
III	Day 0 (N=19)	28.3±0.5	28.1±0.6
	Day 26 (N=19)	27.1±0.4	27.3±0.4